SCIENTIFIC REPORTS
nature research

OPEN

A novel hybridity model for TiO_2-CuO/water hybrid nanofluid flow over a static/moving wedge or corner

Saeed Dinarvand[1], Mohammadreza Nademi Rostami[1] & Ioan Pop[2*]

In this study, we are going to investigate semi-analytically the steady laminar incompressible two-dimensional boundary layer flow of a TiO_2-CuO/water hybrid nanofluid over a static/moving wedge or corner that is called Falkner-Skan problem. A novel mass-based approach to one-phase hybrid nanofluid model that suggests both first and second nanoparticles as well as base fluid masses as the vital inputs to obtain the effective thermophysical properties of our hybrid nanofluid, has been presented. Other governing parameters are moving wedge/corner parameter (λ), Falkner-Skan power law parameter (m), shape factor parameter (n) and Prandtl number (Pr). The governing partial differential equations become dimensionless with help of similarity transformation method, so that we can solve them numerically using bvp4c built-in function by MATLAB. It is worthwhile to notice that, validation results exhibit an excellent agreement with already existing reports. Besides, it is shown that both hydrodynamic and thermal boundary layer thicknesses decrease with the second nanoparticle mass as well as Falkner-Skan power law parameter. Further, we understand our hybrid nanofluid has better thermal performance relative to its mono-nanofluid and base fluid, respectively. Moreover, a comparison between various values of nanoparticle shape factor and their effect on local heat transfer rate is presented. It is proven that the platelet shape of both particles ($n_1 = n_2 = 5.7$) leads to higher local Nusselt number in comparison with other shapes including sphere, brick and cylinder. Consequently, this algorithm can be applied to analyze the thermal performance of hybrid nanofluids in other different researches.

Nanofluids categorize as solid-liquid mixtures including a carrier medium namely base fluid and nano-size particles. Because of very small dimensions (1–100 nm) and huge specific surface area of the nanoparticles, nanofluids have good thermophysical properties; accordingly, they can be used widely in various aspects of technology consisting of microelectromechanical system (MEMS) and nanotechnologies. It is conventional that the thermal conductivity of nanoparticles, especially, metals, their oxides, graphite, and its derivatives exceeds by several orders the thermal conductivity of traditional working fluids (e.g. water, propylene glycol and different oils). Applying a liquid with dispersed particles as the heat-transfer fluid was started a long time ago; however, the classical scattered liquids cannot apply due to sedimentation of the dispersed particles. Nanofluids do not possess foregoing disadvantages. The first experiments of the nanofluids thermal conductivity have elucidated perfect results: the use of nanoparticles (metals or their oxides) in very small volume fractions significantly enhanced the thermal conductivity of the base fluid. So, these new working fluids may be used in many heat transfer applications, like engine cooling, refrigeration, cooling electronics, solar water heating, thermal storage, and so forth (Aliofkhazraei[1]). Although there are some inconsistencies in the previously published literature and incompliance behaviors of the mechanism of the heat transfer in nanofluids, it has known as an efficient heat transfer fluid. It is worth mentioning that many works on nanofluids can be discovered in the useful books by Das *et al.*[2], Nield and Bejan[3], Minkowycz *et al.*[4], and Shenoy *et al.*[5], in the review articles by Buongiorno *et al.*[6], Kakaç and Pramuanjaroenkij[7], Manca *et al.*[8], Mahian *et al.*[9], Sheikholeslami and Ganji[10], Myers *et al.*[11], as well as in the research articles by Mehryan *et al.*[12], Mohebbi *et al.*[13], Dinarvand *et al.*[14], Abedini *et al.*[15], Esfe *et al.*[16], Nademi Rostami *et al.*[17], etc. These reviews illustrate in details, the preparation methods of nanofluids, theoretical and

[1]Department of Mechanical Engineering, Islamic Azad University, Central Tehran Branch, Tehran, Iran. [2]Department of Mathematics, Babeş-Bolyai University, 400084, Cluj-Napoca, Romania. *email: ipop@math.ubbcluj.ro

empirical findings of thermal conductivity and viscosity of nanofluids, and the mathematical formulation related to convective transport in nanofluids, while research ones study the analytic modeling of single-particle nanofluids or hybrid nanofluids in various complex geometries with the use of single-phase model. This single-phase model is based on Tiwari–Das (see Tiwari and Das[18]) nanofluid model. The foregoing model is valid when there is no relative velocity between the base fluid and the nanoparticles. As a result, we have total thermal equilibrium inside the working fluid including fluid phase and solid phase and therefore, the volume concentration of the nanoparticles will be constant in all points of the bulk fluid. On the other hand, the Tiwari–Das model considers the effective thermophysical properties of the single-phase nanofluid for the dimensional governing partial differential equations, while the only thermophysical property pertaining to similarity variables i.e. kinematic viscosity relates to the base fluid.

Recently, the scientists have also attempted to apply hybrid nanofluids, which are designed by dispersing different nanoparticles either in mixture or composite form (Ranga *et al.*[19]). Applying hybrid nanofluids causes the significant modification in heat transfer and pressure drop specifications by trade-off between advantages and disadvantages of individual suspension, attributed to better aspect ratio, suitable thermal network and especially synergistic influence of nanoparticles. However, the long-term stability, manufacture process, the choice of good nanoparticles combination to get synergistic influence and the expense of nanofluids may be biggest challenges and even beyond the practical applications (Minea[20]). In the last years, the improved heat transfer specifications of the hybrid nanofluids draw the attention of investigators to examine the effect of different nanocomposites in different heat transfer fields, such as heat exchanger (Harandi *et al.*[21]), heat sink (Nimmagada and Venkatasubbaiah[22]), solar collectors (Xuan *et al.*[23], Rativa and Gómez-Malagón[24]), boiling (Bhosale and Borse[25]), micro power generation (He *et al.*[26]), etc. Madhesh *et al.*[27] utilized water-based copper–titania hybrid nanofluids, under particle loading ranging from 0.1% to 2% to study the heat transfer characteristics in a shell-and-tube heat exchanger. Besides, the thermal conductivity of the Al_2O_3/water, CuO/water and Al_2O_3–CuO/water hybrid nanofluid for different temperatures and volume concentrations experimentally investigated by Senthilraja *et al.*[28]. In addition, we mention the review paper by Sarkar *et al.*[29] and the articles by Ghalambaz *et al.*[30,31] on hybrid nanoparticles as additives. It should be mentioned here that, the theoretical simulation of single-phase hybrid nanofluids can be applied by the Tiwari–Das model, too. However, we must initially expand the effective thermophysical properties of mono-nanofluids for hybrid nanofluids with two different nanoparticles. This action has been done before by many researchers like Nademi Rostami *et al.*[17]

Falkner–Skan (see Falkner and Skan[32]) similarity boundary-layer problem discusses streaming flows over (static) wedges with arbitrary angle. The Blasius problem is related to the zero angle and the Heimenz problem is related to the 90° angle for a 2D stagnation point (Panton[33], Tamim *et al.*[34] and Dinarvand *et al.*[35]). There are so many works in literature remarked as "Falkner-Skan" problem. For example see Cebeci and Keller[36], Riley and Weidman[37], Asaithambi[38], Pantokratoras[39] and Ishak *et al.*[40]. The steady boundary-layer flow of a non-Newtonian fluid, implemented by a power-law model, over a moving wedge in a moving fluid is investigated by Ishak *et al.*[41]. Yacob *et al.*[42,43] numerically investigated the steady two-dimensional boundary layer flow over a static/moving wedge immersed in nanofluids with uniform surface temperature and prescribed surface heat flux, respectively. Recently, Nadeem *et al.*[44] studied the characteristics of induced magnetic field incorporated in a viscous fluid past a static/moving wedge with considering Cu, Al_2O_3 and TiO_2 as the nanoparticles and water as the base fluid. He mentioned that the fluid flow caused by a moving wedge is a remarkable problem in which the fluid and wall velocities are proportional each other, this is useful in the thermal processing of sheet-like substance that is a necessary operation in the paper procurement, wire drawing, drawing of plastic films, polymeric sheets and metal spinning.

According to author's knowledge, there is no work on the Falkner-Skan problem with considering hybrid nanofluids yet. As a result, we present the problem of boundary layer flow past a static/moving wedge immersed in water-based hybrid nanofluid with constant surface temperature by a mass-based computational algorithm. This algorithm proposes the new definition of an equivalent solid volume fraction, solid density and solid specific heat at constant pressure that are obtained from thermophysical properties of both base fluid and nanoparticles, simultaneously. Then, foregoing parameters along with other relevant governing parameters are substituting into the governing dimensionless ODEs after implementing similarity variables and numerically solved by bvp4c routine. Moreover, the effect of nanoparticles shape factor is considered, too.

Problem Description and Governing Equations

Assume an incompressible laminar steady two-dimensional boundary layer flow over a static or moving wedge in an aqueous hybrid nanofluid with prescribed external flow and moving wedge velocities as displayed in Fig. 1. We have chosen titania (TiO_2) and copper oxide (CuO) as nanoparticles with water as base fluid. We also assume that the base fluid and nanoparticles are in thermal equilibrium and no slip occurs between them. It is worth mentioning that, to develop the targeted hybrid nanofluid TiO_2-CuO/water, titania is initially dispersed into base fluid then, copper oxide is scattered in TiO_2/water nanofluid. Therefore, the subscript (1) corresponds to first nanoparticle (TiO_2), while subscript (2) is applied for second nanoparticle (CuO) as well as subscript (f) related to base fluid. Table 1 shows thermophysical properties of the base fluid and the nanoparticles at 25 °C (see Dinarvand and Pop[45], Nayak *et al.*[46], Vajjha *et al.*[47]).

According to Fig. 1, we choose 2D Cartesian coordinate system (x, y) where x and y are the coordinates measured along the surface of the wedge and normal to it, respectively. It is assumed that the free stream velocity is $U(x) = U_\infty x^m$ and the temperature of the ambient hybrid nanofluid is T_∞, while the moving wedge velocity is $u_w(x) = U_w x^m$ and its constant temperature surface is T_w. After using boundary layer approximations and Tiwari-Das nanofluid model (see Tiwari and Das[18]) as well as the Bernoulli's equation in free stream, the governing non-linear PDEs of mass, momentum and energy can be written as follows (see Yacob *et al.*[42]):

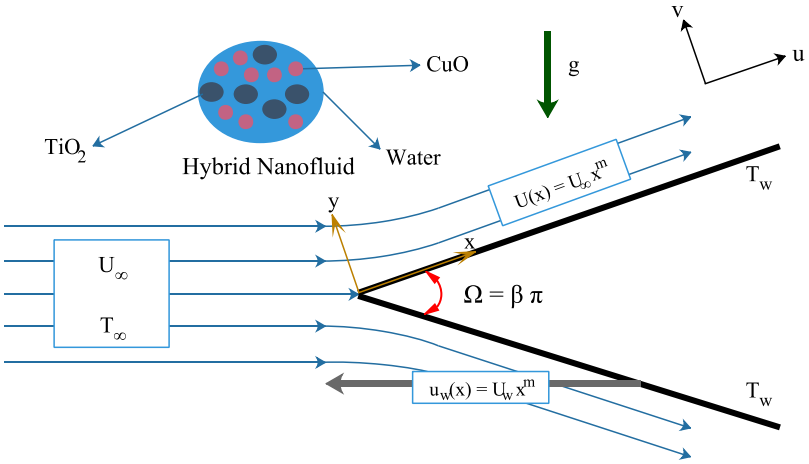

Figure 1. The schematic diagram of the problem and coordinate system.

Thermophysical properties	Pure water (H_2O)	Titania (TiO_2)	Copper oxide (CuO)
C_p(J/kg.K)	4179	686.2	533
ρ(kg/m^3)	997.1	4250	6500
k(W/m. K)	0.613	8.9538	17.65
Particle size (nm)	—	50	29

Table 1. Thermophysical properties of the base fluid and the nanoparticles at 25 °C (Dinarvand and Pop[45], Nayak *et al.*[46] and Vajjha *et al.*[47]).

Property	Hybrid Nanofluid
Viscosity (μ)	$\frac{\mu_f}{(1-\phi)^{2.5}}$
Density (ρ)	$(1-\phi)(\rho_f)+\phi(\rho_s)$
Heat capacity(ρC_p)	$\left[(1-\phi)(\rho_f)+\phi(\rho_s)\right]\times\left[(1-\phi)(C_p)_f+\phi(C_p)_s\right]$
Thermal conductivity (k)	$\frac{k_2+(n_2-1)k_{nf}-(n_2-1)\phi_2(k_{nf}-k_2)}{k_2+(n_2-1)k_{nf}+\phi_2(k_{nf}-k_2)}\times\frac{k_1+(n_1-1)k_f-(n_1-1)\phi_1(k_f-k_1)}{k_1+(n_1-1)k_f+\phi_1(k_f-k_1)}\times(k_f)$
Diffusivity (α)	$\frac{k_{hnf}}{(\rho C_p)_{hnf}}$

Table 2. Applied models for thermophysical properties of the hybrid nanofluid (Sundar *et al.*[48], Ghadikolaei *et al.*[49] and Hayat and Nadeem[50]).

$$\frac{\partial u}{\partial x}+\frac{\partial v}{\partial y}=0, \tag{1}$$

$$u\frac{\partial u}{\partial x}+v\frac{\partial u}{\partial y}=U\frac{dU}{dx}+\frac{\mu_{hnf}}{\rho_{hnf}}\frac{\partial^2 u}{\partial y^2}, \tag{2}$$

$$u\frac{\partial T}{\partial x}+v\frac{\partial T}{\partial y}=\alpha_{hnf}\frac{\partial^2 T}{\partial y^2}, \tag{3}$$

subject to the boundary conditions

$$\begin{aligned} u=u_w(x), \quad v=0, \quad T=T_w \quad at \quad y=0,\\ u\to U(x) \quad T\to T\infty \quad as \quad y\to\infty. \end{aligned} \tag{4}$$

In which u and v are the velocity components along x and y directions, respectively, T is the temperature of the hybrid nanofluid within the thermal boundary layer, C_p is the specific heat at constant pressure, ρ_{hnf}, μ_{hnf} and

Shapes of nanoparticle	n
Spherical	3
Brick	3.7
Cylinder	4.9
Platelet	5.7

Table 3. The common values of shape factor of nanoparticles (Sheikholeslami and Shamlooei[51]).

α_{hnf} are the density, the viscosity and the thermal diffusivity of the hybrid nanofluid, respectively, and are defined according to Table 2.

In Table 2, k_{nf} is the thermal conductivity of the single nanoparticle's nanofluid that is computed from Hamilton-Crosser model (see Ghadikolaei *et al.*[49], and Hayat and Nadeem[50])

$$\frac{k_{nf}}{k_f} = \frac{k_1 + (n_1 - 1)k_f - (n_1 - 1)\phi_1(k_f - k_1)}{k_1 + (n_1 - 1)k_f + \phi_1(k_f - k_1)} \tag{5}$$

where n is the empirical shape factor for the nanoparticle and is determined in Table 3,

Moreover, we propose ϕ, ρ_s and $(C_p)_s$ as the equivalent volume fraction for nanoparticles, the equivalent density of nanoparticles and the equivalent specific heat at constant pressure of nanoparticles, respectively, as well as ϕ_1 and ϕ_2 are solid fraction of first and second nanoparticles, respectively, that are calculated from following formulas (see Sundar *et al.*[48,52,53])

$$\rho_s = \frac{(\rho_1 \times w_1) + (\rho_2 \times w_2)}{w_1 + w_2}, \tag{6}$$

$$(C_p)_s = \frac{\{(C_p)_1 \times w_1\} + \{(C_p)_2 \times w_2\}}{w_1 + w_2}, \tag{7}$$

$$\phi_1 = \frac{\frac{w_1}{\rho_1}}{\frac{w_1}{\rho_1} + \frac{w_2}{\rho_2} + \frac{w_f}{\rho_f}}, \tag{8}$$

$$\phi_2 = \frac{\frac{w_2}{\rho_2}}{\frac{w_1}{\rho_1} + \frac{w_2}{\rho_2} + \frac{w_f}{\rho_f}}, \tag{9}$$

$$\phi = \frac{\frac{w_1 + w_2}{\rho_s}}{\frac{w_1 + w_2}{\rho_s} + \frac{w_f}{\rho_f}}. \tag{10}$$

we notice that, w_1, w_2 and w_f are the first nanoparticle, the second nanoparticle and the base fluid masses, respectively.

According to White[54] we are looking for a similarity solution of Eqs (1–3) along with boundary conditions (4) of the following form:

$$\eta = \left(\frac{(m+1)U(x)}{2\nu_f x}\right)^{1/2} y, \quad \psi = \left(\frac{2\nu_f x U(x)}{m+1}\right)^{1/2} f(\eta), \quad \theta(\eta) = \frac{T - T\infty}{T_w - T\infty}, \tag{11}$$

where ψ is the dimensional stream function and is expressed in the usual form as $u = \partial\psi/\partial y$ and $v = -\partial\psi/\partial x$, f is the dimensionless stream function, θ is the dimensionless temperature distribution of the hybrid nanofluid and η is independent similarity variable. Fortunately, using similarity transformation method, substituting Eq. (11) into non-linear PDEs (2) and (3) and considering Eqs (8–10), give us a following set of dimensionless non-linear ODEs:

$$A_1 f''' + ff'' + \frac{2m}{m+1}(1 - f'^2) = 0, \tag{12}$$

$$\frac{1}{Pr}\frac{k_{hnf}}{k_f}A_2\theta'' + f\theta' = 0, \tag{13}$$

$$A_1 = \left(1 - \frac{\frac{w_1+w_2}{\rho_s}}{\frac{w_1+w_2}{\rho_s} + \frac{w_f}{\rho_f}}\right)^{-2.5} \left(1 - \frac{\frac{w_1+w_2}{\rho_s}}{\frac{w_1+w_2}{\rho_s} + \frac{w_f}{\rho_f}} + \frac{\frac{w_1+w_2}{\rho_s}}{\frac{w_1+w_2}{\rho_s} + \frac{w_f}{\rho_f}}\frac{\rho_s}{\rho_f}\right)^{-1}$$

$$A_2 = \frac{(\rho C_P)_f}{\left[\left(1 - \frac{\frac{w_1+w_2}{\rho_s}}{\frac{w_1+w_2}{\rho_s} + \frac{w_f}{\rho_f}}\right)(\rho_f) + \frac{\frac{w_1+w_2}{\rho_s}}{\frac{w_1+w_2}{\rho_s} + \frac{w_f}{\rho_f}}(\rho_s)\right] \times \left[\left(1 - \frac{\frac{w_1+w_2}{\rho_s}}{\frac{w_1+w_2}{\rho_s} + \frac{w_f}{\rho_f}}\right)(C_P)_f + \frac{\frac{w_1+w_2}{\rho_s}}{\frac{w_1+w_2}{\rho_s} + \frac{w_f}{\rho_f}}(C_P)_s\right]}$$

restricted with the boundary conditions

$$f(0) = 0, \qquad f'(0) = \lambda, \qquad \theta(0) = 1, \tag{14}$$

$$f'(\infty) \to 1, \qquad \theta(\infty) \to 0. \tag{15}$$

Here, the Prandtl number (Pr), the constant moving wedge parameter (λ) as well as the Hartree pressure gradient parameter (β) are defined as

$$\lambda = \frac{U_w}{U_\infty}, \quad \beta = \frac{2m}{m+1}, \quad Pr = \frac{\upsilon_f}{\alpha_f}, \tag{16}$$

It should be mentioned that $\lambda > 0$ and $\lambda < 0$ correspond to a moving wedge in same and opposite directions to the free stream, respectively, while $\lambda = 0$ corresponds to a static wedge. Furthermore, $\beta > 0$ is caused by negative or favorable pressure gradient, while $\beta < 0$ creates positive or unfavorable pressure gradient (see White[54]).

The skin friction coefficient C_f and the local Nusselt number Nu_x are defined as

$$C_f = \frac{\tau_w}{\rho_f U^2}, \quad Nu_x = \frac{xq_w}{k_f(T_w - T_\infty)}. \tag{17}$$

where, τ_w is the shear stress at the surface of the wedge and q_w is the heat flux from the surface of the wedge, which are illustrated by

$$\tau_w = \mu_{hnf}\left(\frac{\partial u}{\partial y}\right)_{y=0}, \qquad q_w = -k_{hnf}\left(\frac{\partial T}{\partial y}\right)_{y=0}. \tag{18}$$

Finally, after combining Eqs (11), (17) and (18), we obtain

$$\left[\frac{2Re_x}{(m+1)}\right]^{\frac{1}{2}} C_f = \left(1 - \frac{\frac{w_1+w_2}{\rho_s}}{\frac{w_1+w_2}{\rho_s} + \frac{w_f}{\rho_f}}\right)^{-2.5} f''(0), \qquad \left[\frac{2}{(m+1)Re_x}\right]^{\frac{1}{2}} Nu_x = -\frac{k_{hnf}}{k_f}\theta'(0). \tag{19}$$

where $Re_x = Ux/\upsilon_f$ is the local Reynolds number. In summary, we can depict the computational procedure for our new algorithm in Fig. 2.

Results and Discussion

The similarity governing Eqs (12) and (13) along with boundary conditions (14) and (15) are solved numerically for some values of the governing parameters w_1, w_2, w_f, ϕ, ϕ_1, ϕ_2, ρ_s, $(C_p)_s$, λ, m, n_1, n_2 and Pr using the bvp4c built-in function from MATLAB software (see Shampine *et al.*[55]). In this approach, we have considered $4 \leq \eta_\infty \leq 6$, $\Delta\eta = \eta_\infty/100$, and the relative tolerance was set as default (10^{-3}). Needless to say that, we are concentrating on the real (First) solutions that have correct physical reasons.

To validate our numerical procedure, Table 4 shows the value of the similarity skin friction coefficient ($f''(0)$) for pure water ($\phi = \phi_1 = \phi_2 = 0$), static boundary ($\lambda = 0$) and different values of m. We can see from Table 4, with increasing parameter m the similarity skin friction coefficient enhances that it seems reasonable physically. Moreover, Table 5 shows the comparison of the values of the skin friction coefficient $[(2Re_x)/(m+1)]^{1/2} C_f$ and the local Nusselt number $[2/\{(m+1)Re_x\}]^{1/2} Nu_x$ for TiO_2-water nanofluid with different values of $\phi = \phi_1$ and m while $\lambda = 0$(stationary wedge), and $n_1 = n_2 = 3$(Maxwell-Garnet model for k_{hnf}/k_f). Tables 4 and 5 imply that the present results are in good agreement with previous published researches obtained by Yih *et al.*[56], White[54], Ishak *et al.*[40], Yacob *et al.*[42] and Nadeem *et al.*[44].

Hydrodynamic and thermal boundary layers. Figure 3 shows the influence of the Falkner-Skan power law parameter (m) and mass of the second nanoparticle (w_2) on the dimensionless velocity and temperature distributions, when $w_1 = 10\ gr$, $w_f = 100\ gr$, $n_1 = n_2 = 3$, $\lambda = 0$ and $Pr = 6.2$. It is worth mentioning that, $m = -0.0825$ ($\beta = -0.18$) corresponds to corner flow case before separation point, $m = 0$ ($\beta = 0$) corresponds to flat plate case, $m = 0.2$ ($\beta = 1/3$) corresponds to wedge flow case with $\Omega = 60°$ and $m = 1$ ($\beta = 1$) corre-

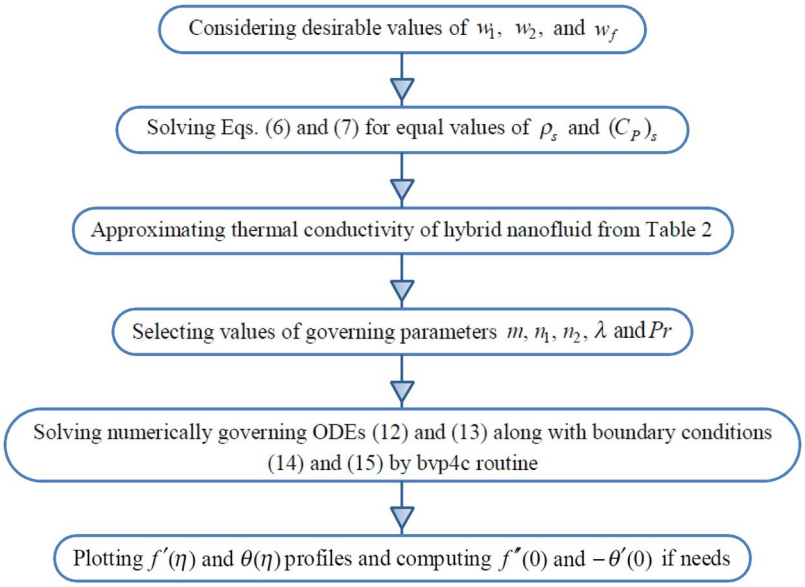

Figure 2. Flowchart of the present problem's computational procedure.

m	Yih *et al.*[56]	White[54]	Ishak *et al.*[40]	Yacob *et al.*[42]	Nadeem *et al.*[44]	Present Study
−0.0825	—	0.12864	—	—	—	0.129310
0	0.469600	—	0.4696	0.4696	0.469600	0.469600
1/11	0.654979	—	0.6550	0.6550	0.654994	0.654993
0.2	0.802125	—	0.8021	0.8021	0.802125	0.802125
1/3	0.927653	—	0.9277	0.9277	0.927680	0.927680
0.4	—	—	—	—	0.976824	0.976824
0.5	—	—	—	1.0389	1.038900	1.038903
1	1.232588	1.23259	1.2326	1.2326	1.232587	1.232587

Table 4. The values of $f''(0)$ for various values of m, when $\phi = \phi_1 = \phi_2 = \lambda = w_1 = w_2 = 0$, $w_f = 100\ gr$ and $Pr = 6.2$.

			$[(2Re_x)/(m+1)]^{1/2}C_f$		$[2/\{(m+1)Re_x\}]^{1/2}Nu_x$	
m	$\phi = \phi_1$	ϕ_2	Yacob *et al.*[42]	Present Study	Yacob *et al.*[42]	Present Study
0	0.1	0	0.6169	0.616929	1.0189	1.018845
	0.2	0	0.7978	0.797872	1.1561	1.156053
0.5	0.1	0	1.3648	1.364842	1.2460	1.246064
	0.2	0	1.7651	1.765142	1.4082	1.408206
1	0.1	0	1.6192	1.619291	1.3010	1.301085
	0.2	0	2.0942	2.094220	1.4691	1.469032

Table 5. The values of $[(2Re_x)/(m+1)]^{1/2}C_f$ and $[2/\{(m+1)Re_x\}]^{1/2}Nu_x$ for various values of m and $\phi = \phi_1$ (TiO_2-water nanofluid) when $\lambda = 0$, $n_1 = n_2 = 3$ and $Pr = 6.2$.

sponds to plane stagnation point flow case. It can be concluded that, with increasing m and w_2 both hydrodynamic and thermal boundary layer thicknesses decrease. So, the velocity as well as the temperature gradients enhance and according to Eqs (17) and (18) the skin friction coefficient and the local Nusselt number increase. Moreover, the effect of m is comparatively less in dimensionless temperature profiles at fixed w_2 because m does not appear directly in the similarity energy Eq. (13). Figure 4 represents the aforementioned profiles for different values of λ, when $w_1 = 10\ gr$, $w_2 = 30\ gr$, $w_f = 100\ gr$, $n_1 = n_2 = 3$, $m = 0.2$ and $Pr = 6.2$. As a result of this Figure, when the wedge moves in same direction to the free stream ($\lambda > 0$), both hydrodynamic and thermal boundary layer thicknesses are thinner than the static wedge ($\lambda = 0$) and moving wedge in opposite direction to the free stream ($\lambda < 0$). So, the local Nusselt number is higher for moving wedges in same direction to the free stream ($\lambda > 0$).

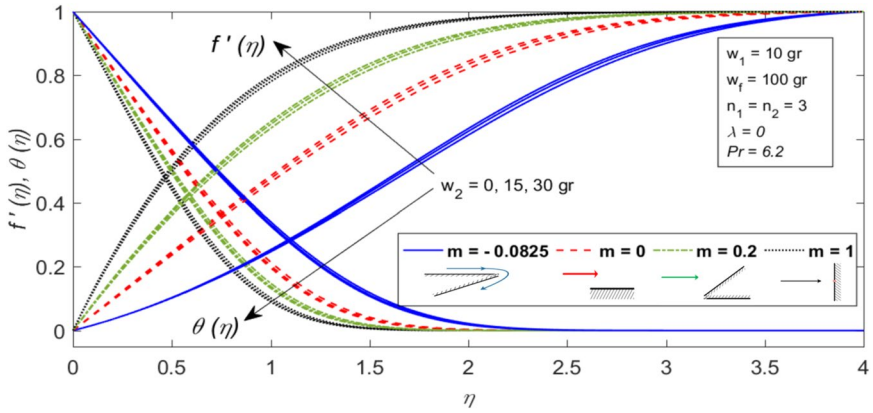

Figure 3. Dimensionless velocity profiles ($f'(\eta)$) and temperature profiles ($\theta(\eta)$) in terms of dimensionless distance from the surface (η) for different values of m and w_2, when $w_1 = 10\ gr$, $w_f = 100\ gr$, $n_1 = n_2 = 3$, $\lambda = 0$ and $Pr = 6.2$.

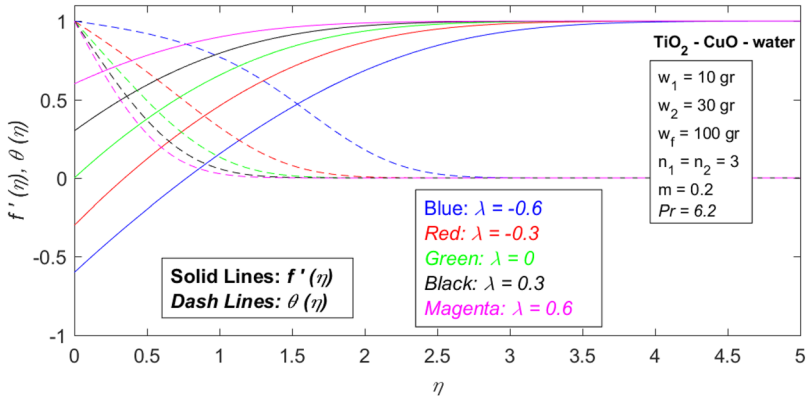

Figure 4. Dimensionless velocity profile ($f'(\eta)$) and temperature profiles ($\theta(\eta)$) in terms of dimensionless distance from the surface (η) for different values of λ, when $w_1 = 10\ gr$, $w_2 = 30\ gr$, $w_f = 100\ gr$, $n_1 = n_2 = 3$, $m = 0.2$ and $Pr = 6.2$.

Engineering quantities of interest: skin friction coefficient and Nusselt number. Here, we compare the skin friction coefficient $[(2Re_x)/(m+1)]^{1/2}C_f$ and the local Nusselt number $[2/\{(m+1)Re_x\}]^{1/2}Nu_x$ in terms of different values of first and second nanoparticle's mass in Figs 5 and 6, respectively, by considering $n_1 = n_2 = 3$, $\lambda = -0.4$, $m = 0.2$ and $Pr = 6.2$.

It is quite clear that, both the skin friction coefficient (the undesirable effect) and the local Nusselt number (the desired effect) increase with increasing first and second nanoparticle masses for all cases. Indeed, increasing the nanoparticles mass leads to augmenting the effective thermal conductivity, and consequently tends the heat transfer rate enhancement of our heat transfer fluid. On the other hand, according to Eq. (19), the most important factors affecting the skin friction coefficient enhancement are (i) the first and second nanoparticles as well as the base fluid masses (w_1, w_2 and w_f) and (ii) the absolute values of the dimensionless velocity profile's slope at the surface of the wedge ($f''(0)$). As a result, the skin friction coefficient enhancement always can occur by net increase of both these factors. In *HNF*4 case, we obtain the largest heat transfer rate ($[2/\{(m+1)Re_x\}]^{1/2}Nu_x = 0.5833$) and also the maximum skin friction coefficient ($[(2Re_x)/(m+1)]^{1/2}C_f = 1.1974$) between all cases that means it has better heat transfer rate relative to single nanoparticle's nanofluid as well as pure water. So, the best status would be theoretically related to *HNF*4 case. Because in addition to having a 35% growth in heat transfer rate relative to pure water, it has a 36% increase in the skin friction coefficient. While *HNF*1, *HNF*2 and *HNF*3, respectively, have an increase in skin friction coefficient of about 17, 26, and 27%, compared to the base fluid. Nevertheless, checking the optimal range for these mass-based cases will require further field studies in the future. However, our major challenge is the high skin friction that requires the high pressure drop and the high relevant pumping power. Therefore, we always should control this issue for practical applications. After all, we can deduce that hybrid nanofluids sufficiently can be used in all applications where ever single nanoparticle's nanofluids have been used.

Influence of nanoparticles shape on thermal characteristics of problem. Figure 7 demonstrates dimensionless temperature profiles for some values of nanoparticle's shape factor ($n_1 = n_2$) that were exhibited in Table 3, when $w_1 = 10\ gr$, $w_2 = 30\ gr$, $w_f = 100\ gr$, $\lambda = -0.4$, $m = 0.2$ and $Pr = 6.2$. As we know, the nan-

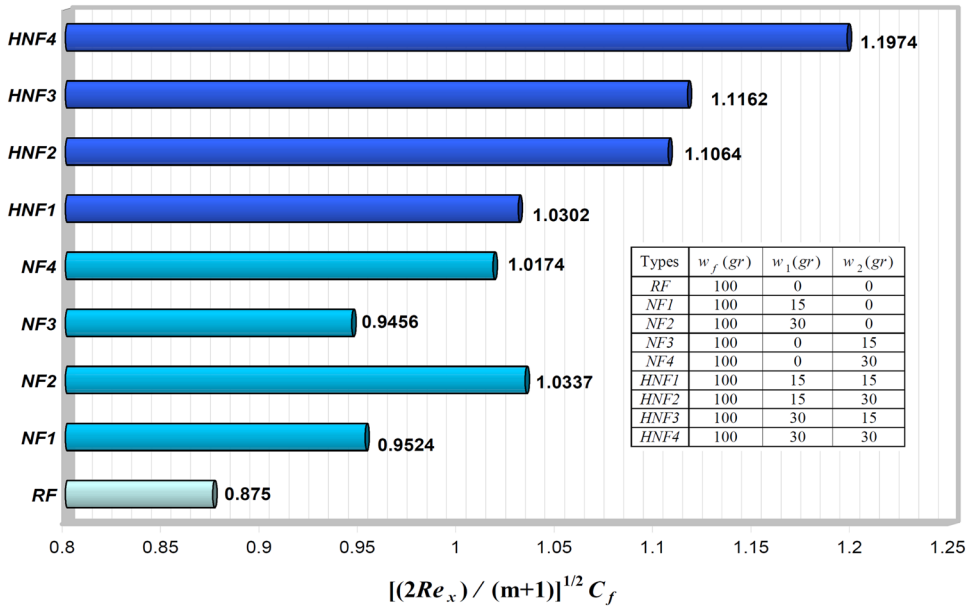

Types	$w_f\,(gr)$	$w_1\,(gr)$	$w_2\,(gr)$
RF	100	0	0
NF1	100	15	0
NF2	100	30	0
NF3	100	0	15
NF4	100	0	30
HNF1	100	15	15
HNF2	100	15	30
HNF3	100	30	15
HNF4	100	30	30

Figure 5. The skin friction coefficient $[(2Re_x)/(m+1)]^{1/2} C_f$ for various values of w_1 and w_2, when $w_f = 100\ gr$, $n_1 = n_2 = 3, \lambda = -0.4, m = 0.2$ and $Pr = 6.2$.

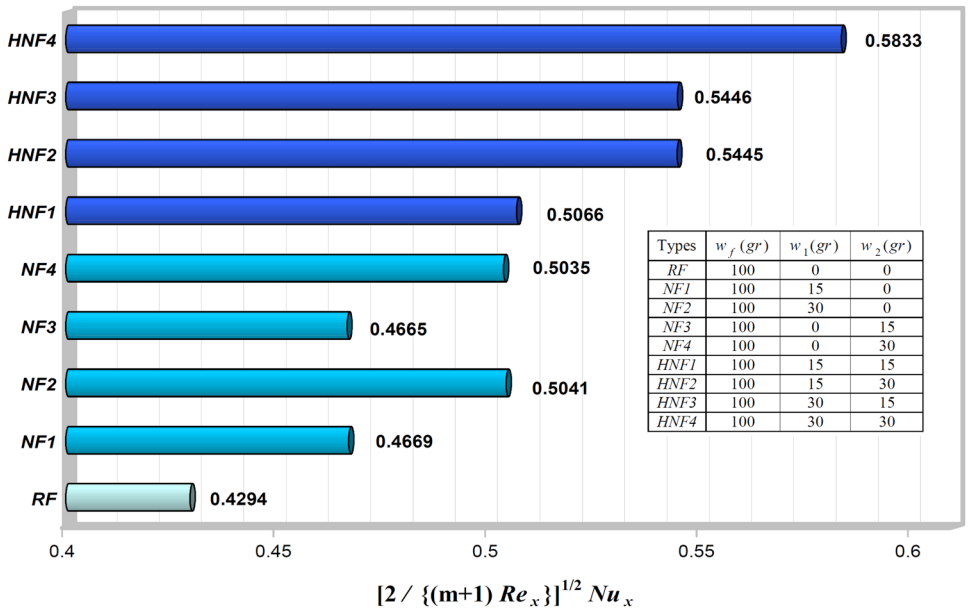

Types	$w_f\,(gr)$	$w_1\,(gr)$	$w_2\,(gr)$
RF	100	0	0
NF1	100	15	0
NF2	100	30	0
NF3	100	0	15
NF4	100	0	30
HNF1	100	15	15
HNF2	100	15	30
HNF3	100	30	15
HNF4	100	30	30

Figure 6. The local Nusselt number $[2/\{(m+1)Re_x\}]^{1/2} Nu_x$ for various values of w_1 and w_2, when $w_f = 100\ gr$, $n_1 = n_2 = 3, \lambda = -0.4, m = 0.2$ and $Pr = 6.2$.

oparticles shape factor (n_1 and n_2) only affect the thermal characteristics of the problem due to their representations in the similarity energy Eq. (13) (see Eq. (13) and the thermal conductivity approximation of hybrid nanofluid in Table 2). On the other hand, values of local Nusselt number of nanoparticles shape factor from Fig. 7 are depicted in the bar diagram of Fig. 8. It is worth mentioning that, Fig. 8 illustrates when the nanoparticles shape is platelet ($n_1 = n_2 = 5.7$), we possess largest heat transfer rate ($[2/\{(m+1)Re_x\}]^{1/2} Nu_x = 0.5916$) while, the opposite trend is valid for spherical shape of nanoparticles ($n_1 = n_2 = 3$).

Finally, in Table 6 we have compared the local Nusselt number of different shapes of first (TiO_2) and second (CuO) nanoparticles (n_1 and n_2) in terms of different hybrid nanofluid masses that are tabulated in Figs 5 and 6 (entitled *HNF*1-*HNF*4), when $w_f = 100\ gr$, $\lambda = -0.4$, $m = 0.2$ and $Pr = 6.2$. It is seen that the local Nusselt number enhances with elevating shape factor of first or second nanoparticles in all cases. Further, it is perceived that, generally when the shape of second nanoparticle is spherical ($n_2 = 3$) while, the shape of first nanoparticle is not spherical ($n_1 \neq 3$), the heat transfer rate of hybrid nanofluid is higher relative to opposite ones.

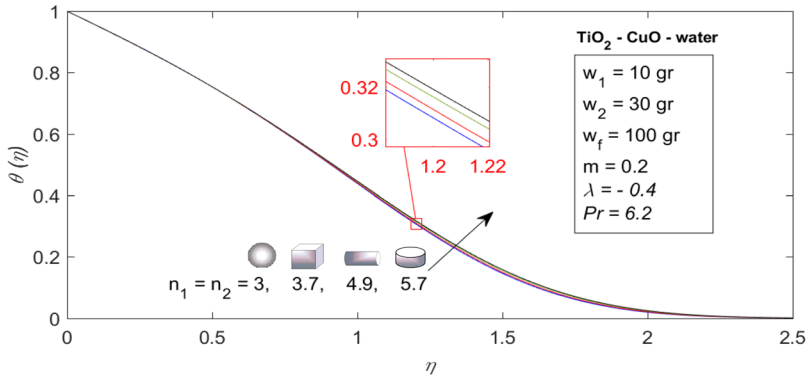

Figure 7. Dimensionless temperature profiles ($\theta(\eta)$) for some values of $n_1 = n_2$ when $w_1 = 10\ gr, w_2 = 30\ gr$, $w_f = 100\ gr, \lambda = -0.4, m = 0.2$ and $Pr = 6.2$.

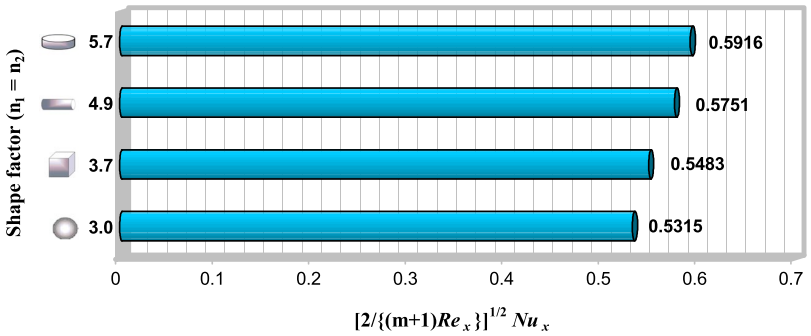

Figure 8. The local Nusselt number $[2/\{(m+1)Re_x\}]^{1/2}Nu_x$ for some values of $n_1 = n_2$, when $w_1 = 10\ gr$, $w_2 = 30\ gr, w_f = 100\ gr, \lambda = -0.4, m = 0.2$ and $Pr = 6.2$.

Types	$n_1 = 3$				$n_2 = 3$			
	$n_2 = 3$	$n_2 = 3.7$	$n_2 = 4.9$	$n_2 = 5.7$	$n_1 = 3$	$n_1 = 3.7$	$n_1 = 4.9$	$n_1 = 5.7$
HNF1	0.5066	0.5125	0.5218	0.5276	0.5066	0.5137	0.5244	0.5308
HNF2	0.5445	0.5565	0.5757	0.5876	0.5445	0.5520	0.5634	0.5702
HNF3	0.5446	0.5508	0.5605	0.5666	0.5446	0.5589	0.5805	0.5933
HNF4	0.5833	0.5959	0.6159	0.6282	0.5833	0.5984	0.6214	0.6349

Table 6. The local heat transfer rate ($[2/\{(m+1)Re_x\}]^{1/2}Nu_x$) for some values of n_1 and n_2 based on various cases of hybrid nanofluids mass, when $\lambda = -0.4$, $m = 0.2$ and $Pr = 6.2$.

Conclusions

The laminar two-dimensional Falkner-Skan problem by taking Newtonian TiO_2-CuO/water hybrid nanofluid into account as the working liquid and with constant surface temperature was investigated semi-analytically with help of new proposed algorithm according to nanoparticles and base fluid masses. Our hypothesize was that the Prandtl number of water is 6.2. After implementing Tiwari-Das single-phase nanofluid model, non-dimensional form of the governing PDEs were written using auxiliary similarity variables, then we attempted to numerically solve them by bvp4c function from MATLAB. The major conclusions of this research, may be summarized as follows: (1) the Falkner-Skan power law parameter (m) and the second nanoparticle mass (w_2) increase the local Nusselt number at the surface of the wedge, (2) the local Nusselt number is higher for moving wedges in same direction to the free stream ($\lambda > 0$) relative to static wedges ($\lambda = 0$) as well as moving wedges in opposite direction to the free stream ($\lambda < 0$), (3) mass increment of first and second nanoparticles invoke enhancement on skin friction and local heat transfer rate of our hybrid nanofluid, (4) when the nanoparticle shape is spheric, the local Nusselt number will be minimum than other nanoparticle shapes, (5) the *HNF4* case with highest nanoparticles mass, possesses the largest local heat transfer rate between other mass-based cases, that means it has better thermal performance relative to mono-nanofluid and base fluid, respectively.

Received: 29 June 2018; Accepted: 17 October 2019;
Published online: 08 November 2019

References

1. Aliofkhazraei, M. Handbook of Nanoparticles (Springer, Switzerland, 2016).
2. Das, S. K., Choi, S. U. S., Yu, W. & Pradeep, Y. Nanofluids: Science and Technology (Wiley, New Jersey 2008).
3. Nield, D. A. & Bejan, A. Convection in Porous Media (4th ed.) (Springer, New York, 2013).
4. Minkowycz, E. M., Sparrow, E. M. & Abraham, J. P. (eds). Nanoparticle Heat Transfer and Fluid Flow (CRC Press, Taylor & Francis Group, New York 2013).
5. Shenoy, A., Sheremet, M. & Pop, I. Convective Flow and Heat Transfer from Wavy Surfaces: Viscous Fluids, Porous Media and Nanofluids (CRC Press, Taylor & Francis Group, New York 2016).
6. Buongiorno, J. *et al*. A benchmark study on the thermal conductivity of nanofluids. *J. Appl. Phys.* **106**, 1–14 (2009).
7. Kakaç, S. & Pramuanjaroenkij, A. Review of convective heat transfer enhancement with nanofluids. *Int. J. Heat Mass Transfer* **52**, 3187–3196 (2009).
8. Manca, O., Jaluria, Y. & Poulikakos, D. Heat transfer in nanofluids. Advances in Mechanical Engineering 2010, Article ID 380826 (2010).
9. Mahian, O., Kianifar, A., Kalogirou, S. A., Pop, I. & Wongwises, S. A review of the applications of nanofluids in solar energy. *Int. J. Heat Mass Transfer* **57**, 582–594 (2013).
10. Sheikholeslami, M. & Ganji, D. D. Nanofluid convective heat transfer using semi analytical and numerical approaches: A review. *J. Taiwan Inst. Chem. Engng.* **65**, 43–77 (2016).
11. Myers, T. G., Ribera, H. & Cregan, V. Does mathematics contribute to the nanofluid debate? *Int. J. Heat Mass Transfer* **111**, 279–288 (2017).
12. Mehryan, S. A. M., Kashkooli, F. M., Ghalambaz, M. & Chamkha, A. J. Free convection of hybrid Al_2O_3-Cu water nanofluid in a differentially heated porous cavity. *Adv. Powder Tech.* **28**, 2295–2305 (2017).
13. Mohebbi, R., Izadi, M. & Chamkha, A. J. Heat source location and natural convection in a C-shaped enclosure saturated by a nanofluid. *Phys. Fluids* **29**, 122009–13 (2017).
14. Dinarvand, S., Hosseini, R. & Pop, I. Axisymmetric mixed convective stagnation-point flow of a nanofluid over a vertical permeable cylinder by Tiwari-Das nanofluid model. *Powder Tech.* **31**, 147–156 (2017).
15. Abedini, A., Armaghani, T. & Chamkha, A. J. MHD free convection heat transfer of a water–Fe_3O_4 nanofluid in a baffled C-shaped enclosure. *J. Therm. Analysis and Calorimetry* **103**, 1–11 (2018).
16. Esfe, M. H., Abbasian Arani, A. A., Yan, W.-M. & Aghaei, A. Natural convection in T-shaped cavities filled with water-based suspensions of COOH-functionalized multi walled carbon nanotubes. *Int. J. Mech. Sci.* **121**, 21–32 (2017).
17. Nademi Rostami, M., Dinarvand, S. & Pop, I. Dual solutions for mixed convective stagnation-point flow of an aqueous silica –alumina hybrid nanofluid. *Chinese Journal of Physics* **56**(5), 2465–2478 (2018).
18. Tiwari, R. J. & Das, M. K. Heat transfer augmentation in a two sided lid-driven differentially heated square cavity utilizing nanofluids. *Int. J. Heat Mass Transfer* **50**, 2002–2018 (2007).
19. Ranga Babu, J. A., Kiran Kumar, K. & Srinivasa Rao, S. State-of-art review on hybrid nanofluids. *Renew. Sustain. Energy Rev.* **77**, 551–565 (2017).
20. Minea, A. A. A review on the thermophysical properties of water-based nanofluids and their hybrids. The Annals of "DUNAREA DE JOS" University of GALATI, 083X, 35-47 (2016).
21. Harandi, S. S., Karimipour, A., Afrand, M., Akbari, M. & D'Orazio, A. An experimental study on thermal conductivity of F-MWCNTs-Fe_3O_4/EG hybrid nanofluid: effects of temperature and concentration. *Int. Commun. Heat Mass Transf* **76**, 171–177 (2016).
22. Nimmagadda, R. & Venkatasubbaiah, K. Conjugate heat transfer analysis of microchannel using novel hybrid nanofluids (Al_2O_3 + Ag/water. *Eur. J. Mech. - B/Fluids* **52**, 19–27 (2015).
23. Xuan, Y., Duan, H. & Li, Q. Enhancement of solar energy absorption using a plasmonic nanofluid based on TiO_2/Ag composite nanoparticles. *RSC Adv.* **4**, 16206–16213 (2014).
24. Rativa, D. & Gómez-Malagón, L. A. Solar radiation absorption of nanofluids containing metallic nanoellipsoids. *Sol. Energy* **118**, 419–425 (2015).
25. Bhosale, G. H., Borse, S. L. & Pool Boiling, C. H. F. Enhancement with Al_2O_3-CuO/H_2O Hybrid Nan fluid. Int. J. engineering research &. *technology* **2**(10), 946–950 (2013).
26. He, Y., Vasiraju, S. & Que, L. Hybrid nanomaterial-based nanofluids for micropower generation. *RSC Adv.* **4**, 2433–2439 (2014).
27. Madhesh, D., Parameshwaran, R. & Kalaiselvam, S. Experimental investigation on convective heat transfer and rheological characteristics of Cu-TiO_2 hybrid nanofluids. *Exp. Thermal Fluid Sci.* **52**, 104–115 (2014).
28. Senthilaraja, S., Vijayakumar, K. & Ganadevi, R. A comparative study on thermal conductivity of Al_2O_3/water, CuO/water and Al_2O_3– CuO/water nanofluids. *Digest J. of Nanomaterials and Biostructures* **10**, 1449–1458 (2015).
29. Sarkar, J., Ghosh, P. & Adil, A. A. Review on hybrid nanofluids: Recent research, development and applications. *Renewable & Sustainable Energy Reviews* **43**, 164–177 (2015).
30. Ghalambaz, M., Doostani, A., Izadpanahi, E. & Chamkha, A. J. Phase-change heat transfer in a cavity heated from below: The effect of utilizing single or hybrid nanoparticles as additives. *J. Taiwan Institute Chem. Engineers* **72**, 104–115 (2017).
31. Ghalambaz, M., Sheremet, M. A., Mehryan, S. A. M., Kashkooli, F. M. & Pop, I. Local non-equilibrium analysis of conjugate free convection within a porous enclosure occupied with Ag-MgO hybrid nanofluid. J. Thermal Analysis Calorimetry 2018 (in press).
32. Falkner, V. M. & Skan, S. W. Some approximate solutions of the boundary-layer equations. *Phil. Mag.* **12**, 865–896 (1931).
33. Panton, R. L. Incompressible Flow, (4th ed.) (Wiley, New Jersey, 2013).
34. Tamim, H., Dinarvand, S., Hosseini, R. & Pop, I. MHD mixed convection stagnation-point flow of a nanofluid over a vertical permeable surface: a comprehensive report of dual solutions. *Heat Mass Transfer* **50**, 639–650 (2014).
35. Dinarvand, S., Hosseini, R. & Pop, I. Unsteady convective heat and mass transfer of a nanofluid in Howarth's stagnation point by Buongiorno's model. *Int. J. Num. Methods Heat Fluid Flow* **25**(5), 1176–1197 (2015).
36. Cebeci, T. & Keller, H. B. Shooting and Parallel Shooting Methods for Solving the Falkner-Skan Boundary-Layer Equation. *J. Comp. Physics* **7**, 289–300 (1971).
37. Riley, N. & Weidman, P. D. Multiple solutions of the Falkner-Skan equation for flow past a stretching boundary. *SIAM J. Appl. Math.* **49**, 1350–1358 (1989).
38. Asaithambi, A. A finite-difference method for the Falkner-Skan equation. *Appl. Math. Comput.* **92**, 135–141 (1998).
39. Pantokratoras, A. The Falkner–Skan flow with constant wall temperature and variable viscosity. *Int. J. Thermal Sci.* **45**, 378–389 (2006).
40. Ishak, A., Nazar, R. & Pop, I. Falkner-Skan equation for flow past a moving wedge with suction or injection. *J. Appl. Math. Comput.* **25**, 67–83 (2007).
41. Ishak, A., Nazar, R. & Pop, I. Moving wedge and flat plate in a power-law fluid. *Int. J. Non-Linear Mech.* **46**, 1017–1021 (2011).
42. Yacob, N. A., Ishak, A. & Pop, I. Falkner-Skan problem for a static or moving wedge in nanofluids. *Int. J. Thermal Sci.* **50**, 133–139 (2011).
43. Yacob, N. A., Ishak, A., Nazar, R. & Pop, I. Falkner–Skan problem for a static and moving wedge with prescribed surface heat flux in a nanofluid. *Int. Commun. Heat Mass Transfer* **38**, 149–153 (2011).
44. Nadeem, S., Ahmad, S. & Muhammad, N. Computational study of Falkner-Skan problem for a static and moving wedge. *Sensors and Actuators B* **263**, 69–76 (2018).

45. Dinarvand, S. & Pop, I. Free-convective flow of copper/water nanofluid about a rotating down-pointing cone using Tiwari-Das nanofluid scheme. *Advanced Powder Technology* **28**, 900–909 (2017).
46. Nayak, A. K., Singh, R. K. & Kulkarni, P. P. Measurement of Volumetric Thermal Expansion Coefficient of Various Nanofluids. *Technical Physics Letters* **36**, 696–698 (2010).
47. Vajjha, R. S., Das, D. K. & Kulkarni, D. P. Development of new correlations for convective heat transfer and friction factor in turbulent regime for nanofluids. *Int. J. Heat Mass Transfer* **53**, 4607–4618 (2010).
48. Syam Sundar., L., Sharma, K. V., Singh, M. K. & Sousa, A. C. M. Hybrid nanofluids preparation, thermal properties, heat transfer and friction factor – A review. *Renew. Sustain. Energy Rev.* **68**, 185–198 (2017).
49. Ghadikolaei, S. S., Yassari, M., Sadeghi, H., Hosseinzadeh, K. & Ganji, D. D. Investigation on thermophysical properties of TiO_2–Cu/H_2O hybrid nanofluid transport dependent on shape factor in MHD stagnation point flow. *Powder Technology* **322**, 428–438 (2017).
50. Hayat, T. & Nadeem, S. Heat transfer enhancement with Ag – CuO/water hybrid nanofluid. *Results in Physics* **7**, 2317–2324 (2017).
51. Sheikholeslami, M. & Shamlooei, M. Magnetic source influence on nanofluid flow in porous medium considering shape factor effect. *Physics Letters A* **381**, 3071–3078 (2017).
52. Syam Sundar, L. *et al*. nanofluids: Preparation and measurement of viscosity, electrical and thermal conductivities. Int. *Comm. Heat Mass Transfer* **73**, 62–74 (2016).
53. Syam Sundar, L., Singh, M. K. & Sousa., A. C. M. Enhanced heat transfer and friction factor of MWCNT–Fe_3O_4/water hybrid nanofluids. Int. Comm. *Heat Mass Transfer* **52**, 73–83 (2014).
54. White, F. M. Viscous Fluid Flow (3rd ed.) (McGraw-Hill, New York, 2006).
55. Shampine, L. F., Gladwell, I. & Thompson, S. Solving ODEs with MATLAB (Cambridge University Press, Cambridge 2003).
56. Yih, K. A. Uniform suction/blowing effect on forced convection about a wedge: uniform heat flux. *Acta Mech.* **128**, 173–181 (1998).

Acknowledgements

The work of I. Pop has been supported from the grant PN-III-P4-ID-PCE-2016-0036, UEFISCDI, Romanian Ministry of Sciences. The authors wish to express their thanks to the very competent Reviewers for the valuable comments and suggestions.

Author contributions

I.P. wrote the literature review, the discussions and the interpretation of the results and co-wrote the manuscript. S.D. and M.N.R. proposed the mathematical and the numerical models and conducted the numerical analysis, explained the results and wrote the manuscript. All authors originated the developed problem and reviewed the manuscript.

Competing interests

The authors declare no competing interests.

Additional information

Correspondence and requests for materials should be addressed to I.P.

Reprints and permissions information is available at www.nature.com/reprints.

Publisher's note Springer Nature remains neutral with regard to jurisdictional claims in published maps and institutional affiliations.